We are IntechOpen,
the world's leading publisher of
Open Access books
Built by scientists, for scientists

6,900
Open access books available

185,000
International authors and editors

200M
Downloads

154
Countries delivered to

Our authors are among the

TOP 1%
most cited scientists

12.2%
Contributors from top 500 universities

CLARIVATE ANALYTICS

BOOK
CITATION
INDEX

INDEXED

WEB OF SCIENCE™

Selection of our books indexed in the Book Citation Index
in Web of Science™ Core Collection (BKCI)

Interested in publishing with us?
Contact book.department@intechopen.com

Numbers displayed above are based on latest data collected.
For more information visit www.intechopen.com

Chapter

Investigation of Nonisothermal Combustion Kinetics of Isolated Lignocellulosic Biomass: A Case Study of Cellulose from Date Palm Biomass Waste

Emmanuel Galiwango and Ali H. Al-Marzouqi

Abstract

The efficient and high yielding acid-base and Organosolv methods were studied for cellulose isolation from date palm lignocellulose waste biomass and thereafter analyzed for nonisothermal kinetic and thermodynamic parameter determination using model-free methods. The structural and chemical characterization of the isolated celluloses revealed structures and functional groups characteristics of cellulose. Thermal decomposition analysis revealed one major peak with average mass loss of $72.51 \pm 0.7\%$ and $55.82 \pm 1.1\%$ for the acid-base and Organosolv method, respectively. This occurred in the temperature region between 250 and 350°C associated with cellulose degradation and contrasted with the three peaks detected in the original biomass. The kinetic and thermodynamic results revealed a strong relationship between the average activation energy and average change in enthalpy with a difference of 5.23 and 147.07 kJmol^{-1} for Organosolv and acid-base methods, respectively. The Gibbs's free energy results revealed that Organosolv cellulose pyrolysis would reach equilibrium faster in KAS, Starink and FWO models with average ΔG values of 115.80 ± 36.62, 115.89 ± 36.65, and 119.45 ± 37.98 kJmol^{-1}, respectively. The acid-base method for FWO model gave negative entropy values. The Malek method revealed the acid-base and Organoslv cellulose pyrolysis mechanism as $(g(\alpha) = [-\ln(1-\alpha)]^{\frac{1}{4}})$ and $(g(\alpha) = [-\ln(1-\alpha)]^{\frac{1}{3}})$, characterized by random nucleation and growth, respectively.

Keywords: lignocellulose biomass, nonisothermal kinetics, isolation methods, characterization

1. Introduction

Lignocellulosic biomass is the most abundant, renewable, and one of the cheapest carbon neutral raw materials in the biosphere that can be used to produce sustainable products such as biofuels, using different technologies [1]. The lignocellulosic biomass consists of mainly cellulose carbohydrate polymer, hemicellulose, and the aromatic component, lignin [2]. Lignocellulose biomass can store up to 47

$MJkg^{-1}$ more energy than lithium ion batteries (0.8 $MJkg^{-1}$) [3]. Lignocellulose biomass is considered a potential candidate to sustainable green alternative source of energy and chemicals due to its high energy density, volatile matter content, and global widespread [3]. The release of volatile matter and other contents in biomass has been extensively studied using pyrolysis technology. Pyrolysis involves the conversion of biomass into bio-oil, gases (volatile matter) and biochar, in the absence of oxygen [4, 5]. The technique is robust and essential in providing vital knowledge of kinetics of devolatilization of any biomass prior to further processing via different conversion technologies. In addition, pyrolysis is effective in reducing the bulky biomass into uniform, energy dense, and easily transportable fuel [6]. Despite always being the first stage in most combustion or gasification process, there are no accurate and enough data on the kinetics and reaction mechanisms of different lignocellulosic biomass [7]. This is attributed to the complexity and the varying physico-chemical properties in different lignocellulosic biomass [7]. In addition, there may be many reactions occurring from the extremely complex pyrolysis process of the lignocellulose biomass [8]. Therefore, developing accurate kinetic models to account for all reactions taking place remains a challenge [6]. Isolation of the complex lignocellulosic biomass into individual fractions and characterization of the individual fractions can provide a better understanding of the combustion kinetics and reaction mechanism. Different biomass isolation/extraction techniques such as liquid-liquid, liquid-solid, acid-base, ultrasound, and microwave-assisted extractions, among others, have been reported before [9]. The choice of the method depends on the biomass type and its fraction to be isolated [9]. Hence, each procedure affects the sample's product yields and physical, chemical, kinetic, and thermodynamic properties differently. Despite the studies on the yields and operating parameters such as solvent and time [9], less or no information is available regarding the kinetic and thermodynamic parametric studies for the combustion of the isolated lignocellulose fractions to assess the difference in the extraction processes. Different general kinetic models on lignocellulose biomass have been suggested [10, 11].

Date palm waste constitutes about 500,000 metric tons per year from ca. 44 million date palm trees found in the United Arab Emirates where this research was conducted. The aims of this research are to isolate cellulose from date palm lignocellulose complex using low concentration acid-base solutions and Organosolv techniques and to model nonisothermal combustion kinetics using model-free methods and finally to predict the most probable mechanistic reaction mechanism of the isolated celluloses. Using thermal-gravimetric technique at different heating rates, kinetic and thermodynamic parameters were calculated using model-free methods, namely Kissinger-Akahira-Sunose (KAS), Flynn-Wall-Ozawa (FWO), and Starink models. The FWO model-free method compensates the experimental measurement errors. However, the KAS and Starink methods depend on the choice of good constant degree of conversion from the derivative mass loss function to provide precision of the kinetic data [12]. In addition, application of different model-free methods involves wide conversion range that allows for study of change in mechanism during a reaction and reduces mass transfer limitations by using multiple heating rates [13].

2. Isolation techniques and nonisothermal kinetic studies

The rachis part of adult date palm waste (DPW) (10–15 years old) was supplied by the UAE University farm, Al foah, Al Ain. The samples were ground to 180-micron particle size to reduce the effects of heat and mass transfer limitations. All

the solvents (ACS grade) and reagents were supplied by Sigma Aldrich and were used with no further purification. Prior to cellulose isolation, 10 g biomass was valorized with benzene/ethanol (2, 1 v/v) for 48 h using Soxhlet extraction to reduce extractives such as waxes and resins surrounding the lignocellulose complex.

2.1 Acid-base and Organosolv cellulose isolation methods

For acid-base isolation; DPW (5 g) extractive-free sample of particle size 180 μm was placed in a 250-mL beaker and leached with 200 mL of 0.1 M HCl while heating at 100°C for 2 h under stirring at 150 rpm. After vacuum filtration, the cellulose and lignin-rich residue was washed with 20 mL of deionized water to remove any residual hemicellulose and then air dried overnight. The hemicellulose was solubilized by HCl and heating due to its labile nature making it easy to dissolve out of the lignocellulose complex. The cellulose- and lignin-rich residue was further treated with 200 mL of 0.1 M NaOH while heating at 100°C for 2 h under constant stirring at 150 rpm. After subsequent vacuum filtration of the mixture, the cellulose-rich residue was washed with 20 mL of 0.1 M NaOH to remove any residual lignin. The isolated cellulose was air dried under laboratory conditions overnight prior to characterization.

For Organosolv isolation, DPW were isolated using methanol/water solvents as reported in literature, with some modifications [14]. The 6.7 g sample of particle size 180 μm was placed in high pressure/temperature reactor vessel (Parr 4848, U.S.A). A mixture of 84 mL sulfuric acid (0.045 N), 13.4 mL formaldehyde (37 wt.%), and 84 mL methanol was added to the reactor vessel containing the sample. The reactor was sealed and purged with nitrogen gas (6–10 bars), and the reaction was performed for 1 h at 160°C under constant stirring at 700 rpm. The product mixture was vacuum filtered after cooling to room temperature. The cellulose-rich residues were air dried overnight prior to characterization, and the yield was determined by a gravimetric analysis technique. The ultimate analysis was conducted, and the results are recorded in **Table 1**.

2.2 Fourier transform infrared (FTIR) spectroscopy

The IRTrace-100 FTIR spectrophotometer (Shimadzu, Kyoto, Japan) was used for the FTIR analysis. The extracted celluloses were analyzed to investigate the difference in the functional groups after extraction. The spectral results were recorded within a range of 500–4000 cm^{-1} wavelength using 4 cm^{-1} spectral resolution and 34 scans. **Figure 1** shows several major absorption bands and the difference between the samples. DPW sample before isolation showed typical lignocellulose strong band absorption bonds. For instance, the bands at 1037 cm^{-1}

Proximate and ultimate analyses	Date palm lignocellulose	Organosolv cellulose	Acid-base cellulose
Moisture content (wt.%)	6.72 ± 0.4	7.08 ± 0.4	8.72 ± 0.4
Volatile matter (wt.%)	78.62 ± 0.04	65.22 ± 0.02	66.92 ± 0.01
Ash content (wt.%)	6.12 ± 0.1	7.36 ± 0.04	7.24 ± 0.01
Fixed carbon (wt.%)	5.40 ± 0.01	4.40 ± 0.10	4.80 ± 0.14
HHV (MJkg^{-1})	17.28	15.46	15.18
Cellulose yield (wt.%)	—	43.15 ± 2.40	64.15 ± 2.40

Table 1.
*Physicochemical analysis of biomass (dried basis).*
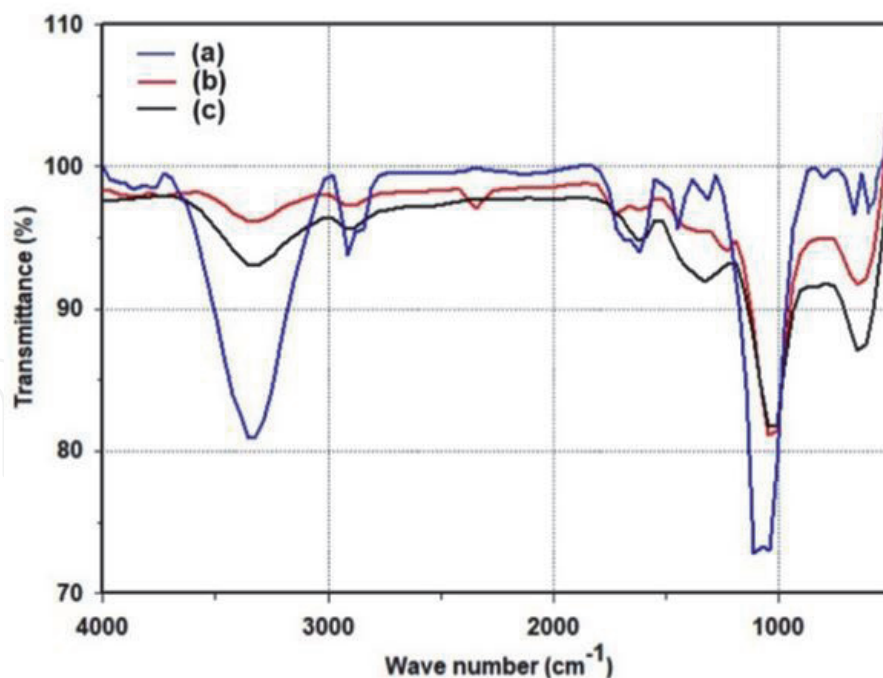
Figure 1.
FTIR spectrum of (a) lignocellulose DPW, (b) Organosolv cellulose and (c) acid-base cellulose.

indicating C—O, C=C and C—C bond stretching, between 2840 and 2926 cm^{-1} indicating C—H stretching and 3200–3474 cm^{-1} for O—H stretching, were assigned to cellulose, hemicellulose and lignin, respectively. Similar results were reported for other biomass in the literature [15]. However, there were noticeable changes in the functional groups of celluloses from the same biomass with reduction in the peak intensity, an indication of component(s) removal (plausibly lignin and hemicellulose). For instance, the would-be lignin and hemicellulose band intensity at 1037 cm^{-1} greatly reduced an indication of component(s) removal. The C—H bond stretching in the region of 2840 assigned to lignin in DPW was absent in isolated cellulose samples. In addition, the reduced peak intensity between 845 and 1156 cm^{-1} associated with the C—O—C asymmetrical stretching and glycosidic bond, a characteristic of cellulose, was observed. Furthermore, the decrease in OH vibration strength around 3200–3474 cm^{-1} indicates a reduction in some of the OH-containing compounds which are phenolics from lignin. It is worth to note that both extraction methods showed similar functional groups except that the Organosolv cellulose had C—H bond assigned to lignin in the region around 2326 and 2363 cm^{-1} which was absent for the acid-base cellulose samples. The FTIR results showed the effectiveness of the cellulose isolation methods from DPW biomass complex. The samples were further characterized for their morphological differences using SEM imaging technique.

2.3 Scanning electron microscopy (SEM)

The structural morphologies of the isolated cellulose were analyzed using the scanning electron microscope (JEOL Neoscope JCM-5000, Tokyo Japan). The samples were Au/C coated using vacuum spatter while clamped on the sample holder. The images were captured on spot size of 40 using 10 kV. The SEM results in **Figure 2** show a difference in the structural morphologies between the cellulose samples from the two methods. **Figure 2(a)** shows the original DPW with ring-like structures (see the arrow point) plausible to be the cellulose chiral nematic ordering, surrounded by irregular shaped structures which could be assumed to be lignin
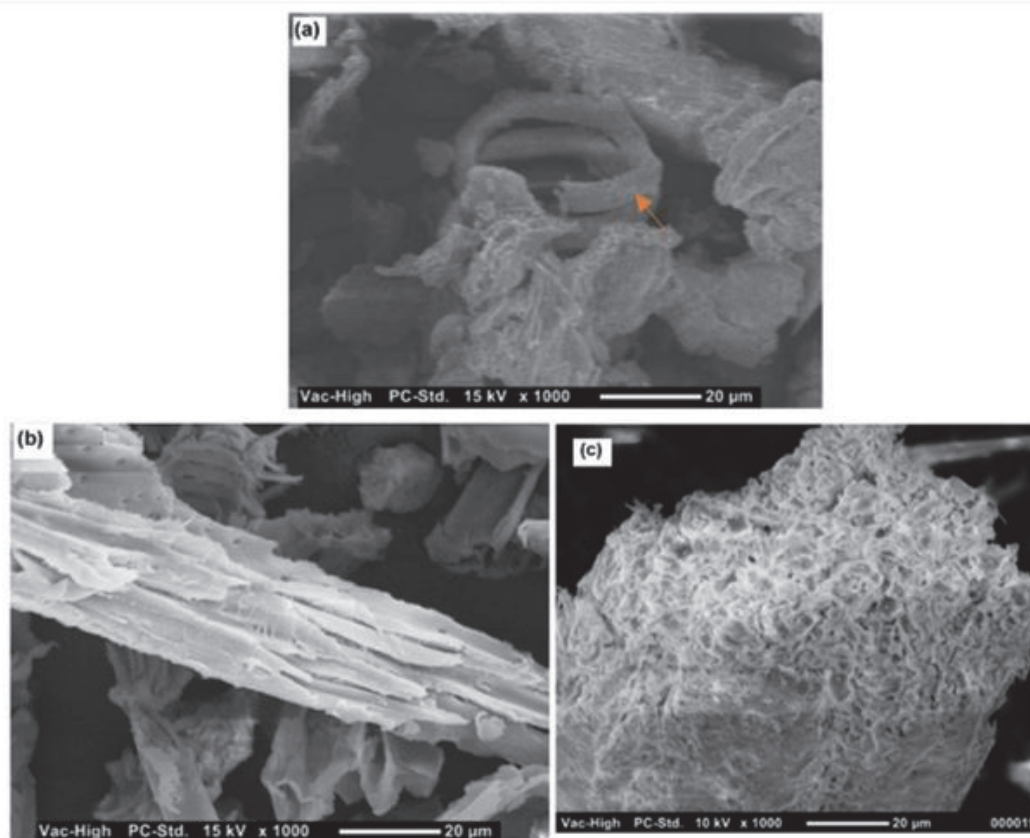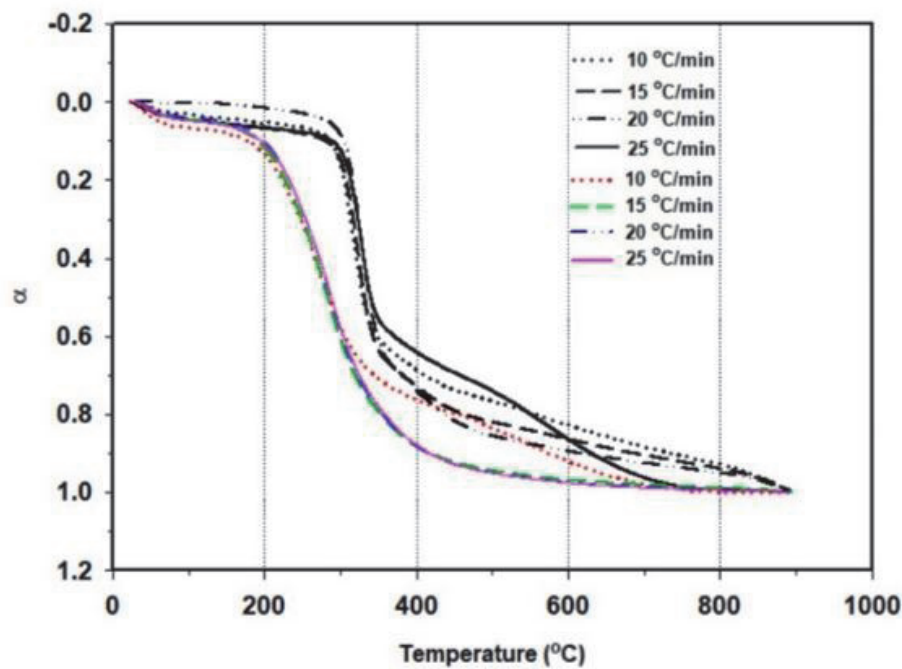
Figure 2.
SEM images of the (a) original rachis, (b) acid-base cellulose and (c). Organosolv cellulose captured at magnification X1000.

and hemicellulose. Acid-base cellulose in **Figure 2(b)** showed porous surface similar to those reported for cellulose from the teak wood [16]. However, Organosolv cellulose (**Figure 2(c)**) showed an aggregate of cellulose block structure with uneven polished surface.

2.4 Thermogravimetric analysis (TGA)

The combustion characteristics of isolated celluloses were studied using thermogravimetric analysis (TGA). The analysis was done on a TGA (Q500, TA instrument). Samples of 6 mg ($\pm$1.0) were first equilibrated at 25°C for 5 min and then heated at specific heating rates of 10, 15, 20, and 25°C/min to 900°C. The process was performed under constant nitrogen environment flowing at 20 mL/min. As the thermal decomposition progressed, the change in weight was recorded continuously as a function of temperature and time. **Figure 3** shows the isoconversion versus temperature at different heating rates for the isolated celluloses from DPW. The conversion curves for acid-base (colored) and Organosolv (black) methods below 300 and 340°C, respectively, showed similar thermal decomposition patterns at all heating rates. There was a slight shift toward higher temperature side with increasing heating rates, possibly due to the increasing thermal energy in the system [17]. However, at higher temperatures, the conversion pattern changed for both methods, possibly due to the change in the degradation chemistry of components under pyrolysis. It is worth to note that Organosolv cellulose showed better thermal stability than the acid-base cellulose. **Figure 4** shows the differential thermogravimetric (DTG) results against temperature at different heating rates for the DPW and the isolated celluloses. The results showed a typical thermal degradation of lignocellulose biomass. The curves of both samples moved downward as the heating

Figure 3.
The relationship of conversion against temperature for acid-base cellulose (colored) and Organosolv cellulose (black).
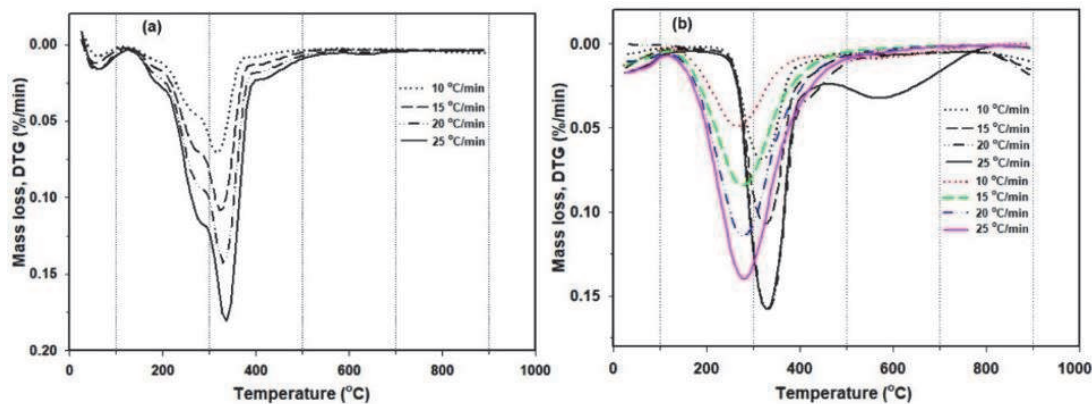
Figure 4.
The relationship of DTG against temperature for (a) date palm waste and (b) isolated celluloses (acid-base, colored; Organosolv, black).

rate increased, owing to the shorter reaction time at increasing temperature, a phenomenon known as thermal hysteresis. However, **Figure 4(a)** showed a noticeable difference between the peak mass loss patterns compared to **Figure 4(b)** for the two cellulose methods, which suggests a difference in the degradation chemistry. **Table 2** shows the temperature ranges that define the major stages of mass loss in response to increasing temperature for isolated celluloses from both methods, as given in **Table 3**. Stage I started from minimum temperature, T_{min} to T_1, the total average celluloses mass loss for acid-base and Organosolv were 9.46 ± 0.1 and $5.28 \pm 0.1\%$, respectively. This was attributed to the inherent moisture and water molecules embedded in the intercellular and intracellular void spaces of the celluloses. Stage II, from T_1 to T_3 for both methods, there was only one major clear peak (**Figure 4(b)**) and the average mass loss in this region was 72.51 ± 0.7 and $55.82 \pm 1.1\%$, for acid-base and Organosolv celluloses, respectively. The weight loss in this stage is associated with pyrolysis of mainly cellulose and to a lesser extent hemicellulose [18]. Compared to the three peaks observed in **Figure 4(a)** for the original DPW, this clearly shows that both methods were effective for cellulose

Heating rate (°C min^{-1})	T_{min} (°C)	T_1 (°C)	T_2 (°C)	T_3 (°C)	T_{max} (°C)
		Acid-base cellulose			
10	30	192	266	402	900
15		197	273	406	
20		199	279	411	
25		201	381	415	
		Organosolv cellulose			
10	30	220	318	422	900
15		226	324	435	
20		227	328	441	
25		228	330	450	

Table 2.
Characteristic temperatures associated with mass loss during pyrolysis of cellulose.

Stages	Temperature	Heating rate (°C min^{-1})			
		10	**15**	**20**	**25**
		Acid-base cellulose			
Stage I, WL%	T_{min}–T_1	10.06	9.17	9.33	9.26
Stage II, WL %	T_1–T_3	71.59	72.76	73.16	72.52
Stage III, WL %	T_3–T_{max}	10.18	8.88	7.30	8.35
Final residue at 900-100 °C (%)		7.99	9.19	11.21	9.87
		Organosolv cellulose			
Stage I, WL %	T_{min}–T_1	4.35	5.24	5.72	5.79
Stage II, WL %	T_1–T_3	54.42	56.16	57.16	55.55
Stage III, WL %	T_3–T_{max}	35.57	33.30	32.24	33.69
Final residue at 900-100 °C (%)		5.66	5.30	4.88	4.97

Table 3.
Mass loss (%) during different stages of cellulose pyrolysis.

isolation from the complex lignocellulose matrix of DPW. Stage III had total average mass loss of 8.68 ± 1.2 and 33.08 ± 0.8%, for acid-base and Organosolv methods, respectively. This represented combustion of the carbonaceous and some part of char oxidation [19]. In addition, the higher mass loss for Organosolv cellulose was plausibly due to residual lignin. Moreover, the FTIR results showed some lignin functional groups for this method. The last stage was associated with charring process and ash formation. The average total mass loss for acid-base and Organosolv methods in this stage were 9.57 ± 1.3 and 5.20 ± 0.4%. TGA analysis data was used for kinetic modeling using the model-free methods.

2.5 Nonisothermal kinetic analysis

The TGA data were used to calculate the nonisothermal kinetic and thermodynamic parameters using model-free equations of Flynn-Wall-Ozawa (FWO), Kissinger-Akahila-Sunose (KAS), and Starink reported in the literature [20].

$$\textit{FWO model}: \ln(\beta) = \ln\left(\frac{AE_\alpha}{g(\alpha)R}\right) - 5.331 - 1.052\left(\frac{-E}{RT}\right) \qquad (1)$$

$$\textit{KAS model}: \ln\left(\frac{\beta_i}{T_{\alpha,i^2}}\right) = \ln\left(\frac{AR}{E_\alpha}\right) - \left(\frac{E_\alpha}{RT_\alpha}\right) + \ln\left(\frac{df(\alpha)}{d\alpha}\right) \qquad (2)$$

$$\textit{Starink model}: \ln\left(\frac{\beta_i}{T_{\alpha,i^{1.92}}}\right) = \ln\left(\frac{AR^{0.92}}{g(\alpha)E_\alpha^{0.92}}\right) - 1.0008\left(\frac{E_\alpha}{RT_\alpha}\right) - 0.312 \qquad (3)$$

where $T_{\alpha,i}$ is the time to reach a given extent of conversion at temperature T_i. At α, the value of E_α is determined from the slope of the plot $\ln(\beta)$, $\ln(\beta/T_{\alpha,i^2})$, and $\ln(\beta/T_{\alpha,i^{1.92}})$ versus $1,000/T_{\alpha,i}$.

$$\alpha = \frac{m_1 - m_t}{m_1 - m_\infty} \qquad (4)$$

where m_1 is the initial biomass weight, m_t is the change in weight at a particular time during the experiment, and m_∞ is the residual weight after time of the experiment.

The choice for these model-free methods is because no previous knowledge about reaction mechanism is required to determine the reaction activation energy [21]. The preexponential factor (A) and thermodynamic parameters [enthalpy (ΔH), entropy (ΔS), and Gibb's free energy (ΔG)] were calculated using equations in literature [22].

$$A = \frac{\left[\beta.\exp\left(\frac{E_\alpha}{RT_m}\right)\right]}{\left[RT_m^2\right]} \qquad (5)$$

$$\Delta H = E_\alpha - RT \qquad (6)$$

$$\Delta G = E_\alpha + RT_m \ln\left(\frac{K_B T_m}{hA}\right) \qquad (7)$$

$$\Delta S = \frac{\Delta H - \Delta G}{T_m} \qquad (8)$$

where β is the heating rate, E_α is the activation energy, T_m is the maximum peak temperature, K_B is the boltzman constant, and h is the plank constant.

The activation energies for both sample methods were calculated using the three models, namely FWO, KAS, and Starink. These model-free methods avoid the shortcomings during model fitting and kinetic compensation effects. The FWO model-free method compensates the experimental measurement errors. However, the KAS and Starink methods depend on the good constant degree of conversion from the derivative mass loss function to provide precision of the kinetic data [12]. Therefore, application of different model-free methods involves a wide conversion range that allows for the study of change in mechanism during a reaction and reduces mass transfer limitations by using multiple heating rates [13]. **Figure 5** shows the relationship of activation energy and enthalpy from the three model-free methods for acid-base and Organosolv celluloses. Results showed little or no differ-ence between E_α and ΔH. This closeness in E_α and ΔH values signifies the formation of activation complex and little extra energy might be required to achieve product formation [23]. Organosolv cellulose E_α and ΔH values were higher than acid-base cellulose especially at higher temperatures ($\alpha > 0.6$). This was possibly due to a
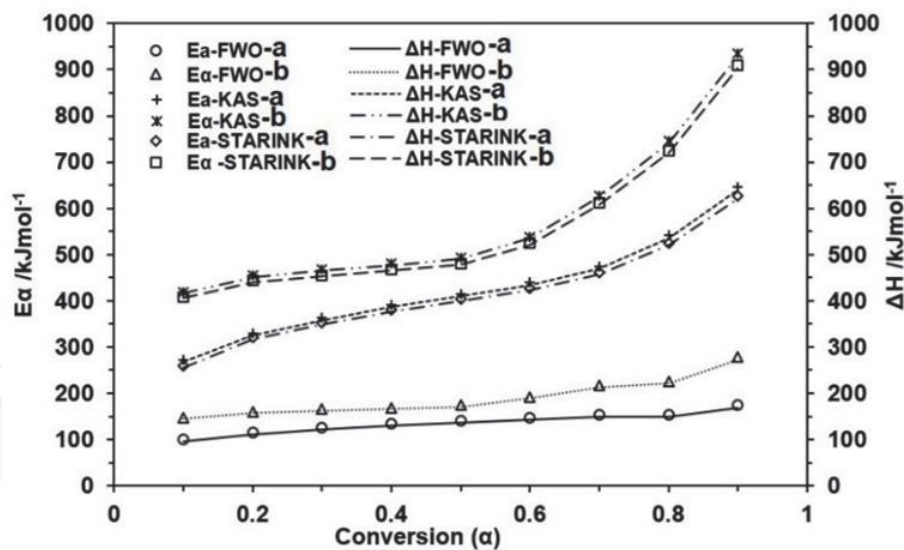
Figure 5.
Activation energy and enthalpies of (a) acid-base cellulose and (b) Organosolv by three model-free methods.

difference in the cellulose structure between the two methods. In addition, the residual lignin fractions detected in Organosolv method could also have resulted in the increased energy of activation, E_α, and bond dissociation, ΔH, needed to overcome the carbon number distribution from other components other than cellulose. It was noted that the ΔH values for all samples were positive, an indication of energy consumed during pyrolysis process, and are used to release various volatile and biochar products. Furthermore, the calculated solid-state process parameters were different due to the fundamental differences in the model-free methods [12, 13]. The first difference arises from the slope, S, of straight lines which is directly proportional to the activation energy, that is, FWO, KAS, and Starink slope, $S = -\frac{1.052E}{RT_\alpha}, S = -\frac{E}{RT_\alpha}$ and $S = -\frac{1.0008E}{RT_\alpha}$, respectively. The second difference is in the time to reach the extent of conversion (T_{α,i^n}) at a given temperature, which is different across different models (for (T_{α,i^n}) term, n = 0, 2, and 1.92 for FWO, KAS, and Starink, respectively).

Tables 4–6 show other thermodynamic parameters from the three model-free methods for the acid-base and the Organosolv cellulose samples, respectively. The ΔG values for Organosolv cellulose for all model-free methods were lower than those of acid-base cellulose samples. Gibb's free energy gives the measure of how favorable a reaction is to reach chemical equilibrium [24]. In context of the first and second laws of thermodynamics, the sample with higher values of ΔG (acid-base cellulose), the further its reaction is from equilibrium and the further its reaction must shift to reach equilibrium. However, the entropy, ΔS values were lower for the acid-base celluloses for all model-free methods, with negative entropy values for the FWO model. This implies that the degree of disorder of initial reactants was higher than that of the products formed by bond dissociations [22]. In addition, it was already discussed previously that the heat input during the thermal decomposition was for bond dissociation of the reactants. In the context of reaction energy, the acid-base cellulose sample required lower activation energy and enthalpy to form products than Organosolv cellulose samples. On the other hand, the preexponential factor of Organosolv cellulose was ca. two times higher than that of acid-base cellulose. This was plausibly because the activation energy had a similar trend as already discussed above. The preexponential factor and activation energy both influence chemical kinetics and reaction dynamics in pyrolysis of biomass involving complex heterogeneous reactions [25]. The R^2 of all model-free parameters was above 0.98, signifying accuracy of the models.

	FWO[a]			FWO[b]		
α	Log A (s⁻¹)	ΔG (kJmol⁻¹)	ΔS (Jmol⁻¹)	Log A (s⁻¹)	ΔG (kJmol⁻¹)	ΔS (Jmol⁻¹)
0.1	10.17	151.46	−0.12	27.20	84.18	0.21
0.2	10.96	164.16	−0.11	27.24	91.96	0.21
0.3	11.34	171.76	−0.10	27.26	94.86	0.21
0.4	11.79	178.07	−0.09	27.15	97.26	0.21
0.5	12.13	183.36	−0.08	27.17	100.17	0.21
0.6	12.25	189.25	−0.08	27.53	109.59	0.21
0.7	12.17	198.03	−0.08	25.07	136.91	0.17
0.8	11.15	216.34	−0.10	21.64	167.53	0.10
0.9	11.28	243.04	−0.10	23.20	192.64	0.13
Av	**11.47 ±0.68**	**188.39 ±27.89**	**−0.10 ±20.01**	**25.94 ± 2.16**	**119.45 ±37.98**	**0.18 ±0.04**

R^2 were above 0.98.
[a]Acid-base.
[b]Organosolv.

Table 4.
The kinetic and thermodynamic parameter values of celluloses determined by FWO model.

	KAS[a]			KAS[b]		
α	Log A (s⁻¹)	ΔG (kJmol⁻¹)	ΔS (Jmol⁻¹)	Log A (s⁻¹)	ΔG (kJmol⁻¹)	ΔS (Jmol⁻¹)
0.1	31.09	138.51	0.28	76.86	81.66	1.16
0.2	34.78	149.86	0.35	76.54	89.24	1.15
0.3	36.56	156.67	0.38	76.62	92.06	1.16
0.4	38.05	162.34	0.41	76.69	94.38	1.16
0.5	39.18	167.12	0.43	76.76	97.21	1.16
0.6	40.29	172.40	0.46	76.72	106.42	1.16
0.7	41.65	180.30	0.48	72.62	132.86	1.08
0.8	43.89	196.73	0.52	71.44	162.07	1.05
0.9	46.97	220.82	0.58	78.19	186.28	1.18
Av	**39.16 ± 4.78**	**171.64 ± 25.07**	**0.43 ± 0.09**	**75.83 ± 2.23**	**115.80 ± 36.62**	**1.14 ± 0.04**

R^2 were above 0.98.
[a]Acid-base
[b]Organosolv.

Table 5.
The kinetic and thermodynamic parameter values of celluloses determined by KAS model.

2.6 Reaction model determination

Malek method which is the commonly used approach to determine probable reaction mechanism involving heterogeneous reaction was used [26]. The Malek method is described by the following equation.

$$Z(\alpha) = f(\alpha)g(\alpha) = \left(\frac{d\alpha}{dt}\right)_\alpha T_\alpha^2 \left[\frac{\Pi(x)}{\beta T_\alpha}\right] \tag{9}$$

	STARINK[a]			STARINK[b]		
α	Log A (s^{-1})	ΔG (kJmol^{-1})	ΔS (Jmol^{-1})	Log A (s^{-1})	ΔG (kJmol^{-1})	ΔS (Jmol^{-1})
0.1	29.65	138.69	0.25	74.89	81.73	1.12
0.2	33.82	149.97	0.33	74.76	89.30	1.12
0.3	35.63	156.78	0.37	74.59	92.13	1.12
0.4	36.99	162.47	0.39	74.71	94.46	1.12
0.5	38.15	167.24	0.41	74.80	97.28	1.12
0.6	39.22	172.53	0.43	74.83	106.50	1.12
0.7	40.55	180.43	0.46	70.70	132.96	1.04
0.8	42.60	196.89	0.50	69.46	162.20	1.01
0.9	45.58	221.00	0.55	76.04	186.43	1.14
Av	38.02 ± 4.75	171.78 ± 25.05	0.41 ± 0.09	73.86 ± 2.21	115.89 ± 36.65	1.10 ± 0.04

R^2 were above 0.98.
[a]Acid-base
[b]Organosolv.

Table 6.
The kinetic and thermodynamic parameter values of celluloses determined by STARINK model.

where $\left(\frac{d\alpha}{dt}\right)_\alpha$ is rate of reaction at a given conversion, α, and heating rate, β, $\Pi(x)$ approximates the temperature integral profile and $x = E_\alpha/RT_\alpha$. The x values used were in a range of 5–20 and the temperature approximation $\Pi(x)$ function is defined by the following equation [27].

$$\Pi(x) = \frac{x^3 + 18x^3 + 88x + 96}{x^4 + 20x^3 + 120x^3 + 240x + 120} \tag{10}$$

The theoretical z(α) plots versus α depend on $f(\alpha)$ and $g(\alpha)$ functions. However, the experimental z(α) values can be obtained by using a specific heating rate for a specific value of $\frac{d\alpha}{dt}$, E_α and T_α. The experimental z(α) master plots as a function of α are compared with known theoretical model functions [28]. The best fit between the experimental z(α) master plots and theoretical model functions describes the probable biomass reaction mechanism. **Figures 6** and **7** show the experimental z(α) master plots and fitted model plots of acid-base and Organosolv, as determined by model-free methods at different heating rates, respectively.
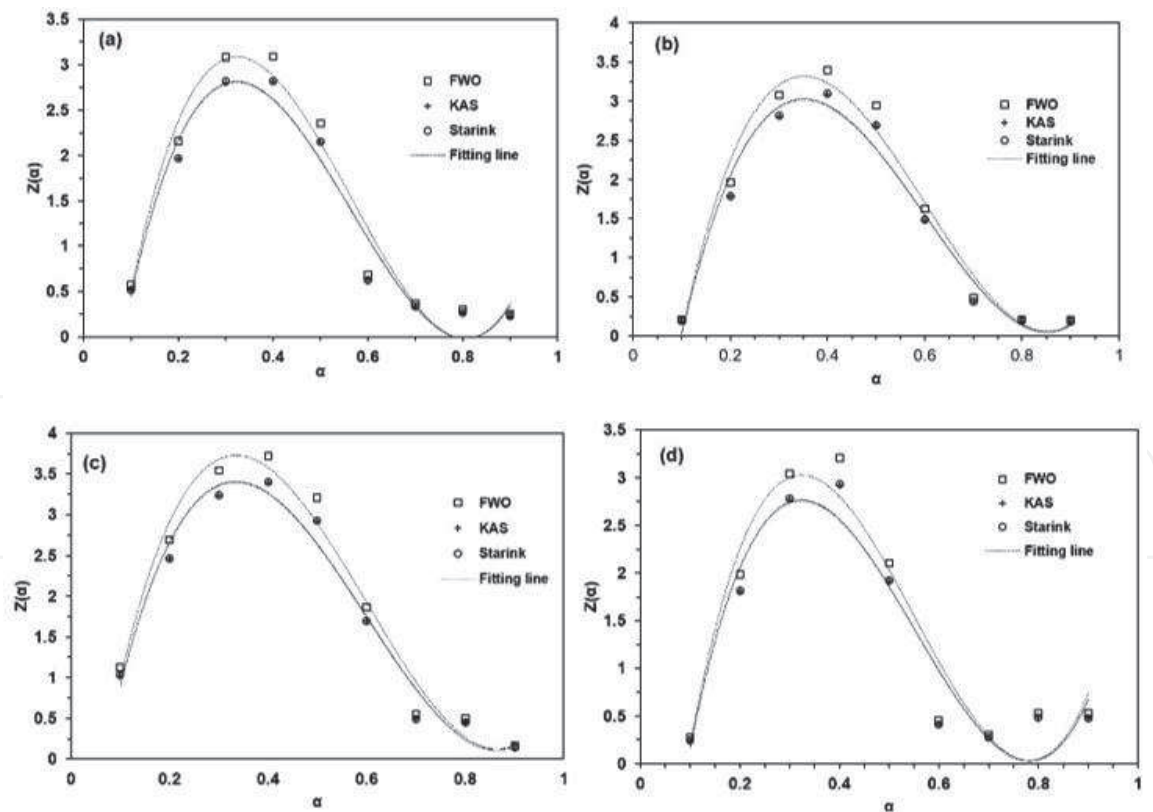
The experimental and the fitted z(α) master plots of acid-base cellulose showed a normal distribution behavioral curve trend for all model-free methods at investigated heating rates. However, Organosolv cellulose showed a sigmoid curve skewed more to the left hand side. The correlation coefficient of acid-base method ranged between 0.9789 and 0.9884, while that of Organosolv ranged between 0.9525 and 0.9795, signifying the accuracy in the reported data. It is worth to note that both methods had best fit at 15°C/min. The data were fit with polynomial curves of n = 3 and n = 4 for Organosolv and acid-base celluloses, respectively, implying third and fourth dimension growth as described by general Avrami-Erofeev model of multidimensional nuclei and random growth reaction mechanism $(g(\alpha) = [-\ln(1-\alpha)]^{\frac{1}{n}})$. This type of mechanism is often as a result of hydration, adsorption, dissolution, and defects on the crystallite within particle size of the
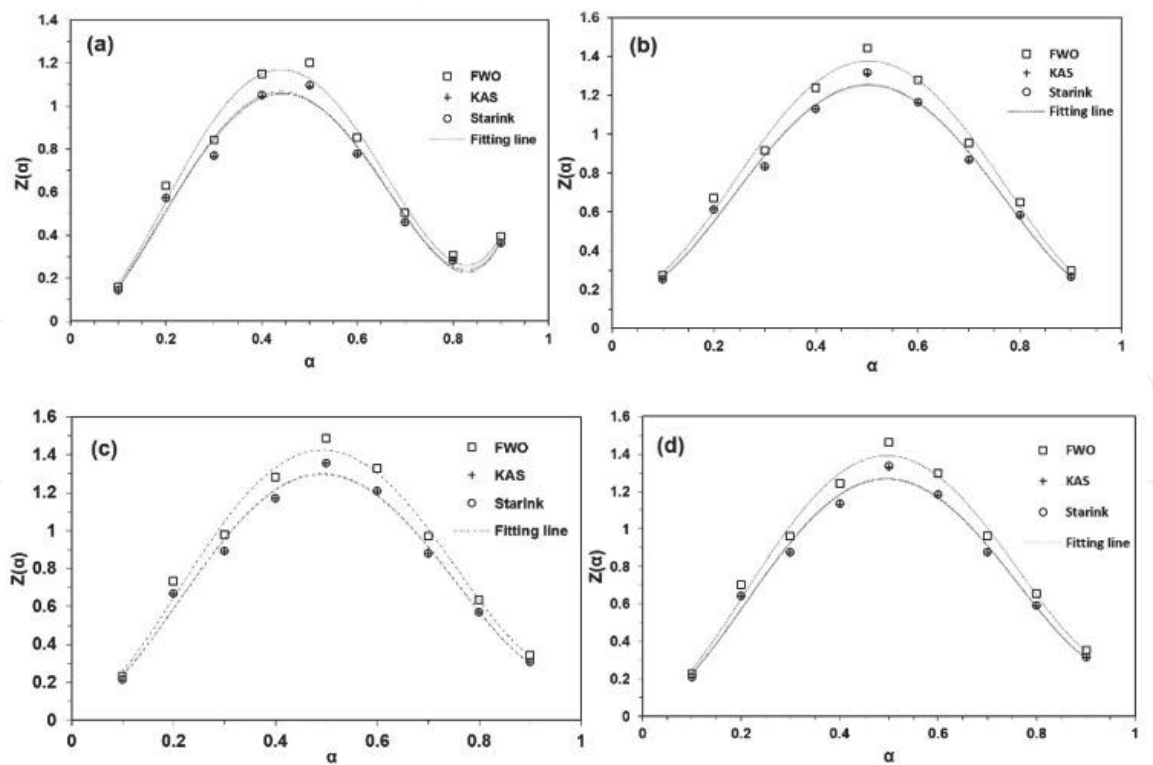
Figure 6.
Experimental and theoretical Z(α) master plots for pyrolysis of acid-base cellulose at (a) $10°Cmin^{-1}$, (b) $15°Cmin^{-1}$, (c) $20°Cmin^{-1}$ and (d) $25°Cmin^{-1}$.

Figure 7.
Experimental and theoretical Z(α) master plots for pyrolysis of Organosolv cellulose at (a) $10°Cmin^{-1}$, (b) $15°Cmin^{-1}$, (c) $20°Cmin^{-1}$ and (d) $25°Cmin^{-1}$.

sample that can cause thermodynamic inhibition leading to varying activation energies [29]. Therefore, random nucleation and growth is the most probable reaction mechanism for the pyrolysis of celluloses isolated from DPW by acid-base and Organosolv methods.

3. Conclusions

The low cost and high yield acid-base and Organosolv methods were assessed for isolation of cellulose from date palm lignocellulose waste biomass. The structural, chemical, and morphological characterizations of the isolated celluloses were studied. The nonisothermal combustion studies were investigated using three different model-free methods. The reaction mechanism was studied using Malek method.

- The SEM images revealed chiral nematic orderings structures distinctive of cellulose. The change in FTIR peak intensity and the difference in the vibrational bond stretching among the isolated celluloses and between original biomass signified component removal from the lignocellulose complex. The TGA results from both methods showed one major decomposition peak assigned to cellulose in contrast to original biomass with three peaks. The results further revealed a possible difference in the degradation chemistry at higher temperature where isoconversion was higher than 0.6.

- The FWO model for the acid-base method gave the lowest activation energy (99.77–173.76 kJmol^{-1}) and the Organosolv method by KAS model gave the highest activation energy (419.63–934.49 kJmol^{-1}). There was a strong relationship between activation energy and enthalpy, and the positive enthalpy values confirmed that endothermic reaction took place during the pyrolysis of the cellulose samples. The Gibbs's free energy, ΔG, results revealed that Organosolv cellulose pyrolysis reaction would easily reach equilibrium, much easier in a trend of KAS > Starink> FWO models. The measure for disorder was less favorable for the acid-base method with negative entropy values in the FWO model-free method.

- The reaction mechanism by Malek method was described by Avrami-Erofeev model mechanism ($g(\alpha) = [-\ln(1-\alpha)]^{\frac{1}{4}}$) for the acid-base method and ($g(\alpha) = [-\ln(1-\alpha)]^{\frac{1}{3}}$) for the Organoslv method.

- The results of this study confirm the existence of multistep mechanism occurring in solid-state reactions due to variations in activation energy with the heating rates. The study provides important data information and a robust approach to understanding the cellulose pyrolysis structures and mechanisms by different isolation methods across a broad range of temperature and different heating rates.

Acknowledgements

Conflict of interest

The authors declare no conflict of interest.

Author details

Emmanuel Galiwango and Ali H. Al-Marzouqi*
United Arab Emirates University, Al Ain, UAE

*Address all correspondence to: hassana@uaeu.ac.ae

IntechOpen

References

[1] Liu C, Wang H, Karim AM, Sun J, Wang Y. Catalytic fast pyrolysis of lignocellulosic biomass. Chemical Society Reviews. 2014;**43**(22):7594-7623

[2] Wu W, Mei Y, Zhang L, Liu R, Cai J. Effective activation energies of lignocellulosic biomass pyrolysis. Energy & Fuels. 2014;**28**(6):3916-3923

[3] Liao JC, Mi L, Pontrelli S, Luo S. Fuelling the future: Microbial engineering for the production of sustainable biofuels. Nature Reviews. Microbiology. 2016;**14**(5):288

[4] Bridgwater AV. Review of fast pyrolysis of biomass and product upgrading. Biomass and Bioenergy. 2012;**38**:68-94

[5] Mohan D, Pittman CU Jr, Steele PH. Pyrolysis of wood/biomass for bio-oil: A critical review. Energy & Fuels. 2006; **20**(3):848-889

[6] Huang L, Ding T, Liu R, Cai J. Prediction of concentration profiles and theoretical yields in lignocellulosic biomass pyrolysis. Journal of Thermal Analysis and Calorimetry. 2015;**120**(2): 1473-1482

[7] Müller-Hagedorn M, Bockhorn H, Krebs L, Müller U. A comparative kinetic study on the pyrolysis of three different wood species. Journal of Analytical and Applied Pyrolysis. 2003; **68**:231-249

[8] Ibbett R, Gaddipati S, Davies S, Hill S, Tucker G. The mechanisms of hydrothermal deconstruction of lignocellulose: New insights from thermal–analytical and complementary studies. Bioresource Technology. 2011; **102**(19):9272-9278

[9] Segneanu A-E, Cziple F, Vlazan P, Sfirloaga P, Grozescu I, Gherman VD. Biomass extraction methods. In: Biomass Now-Sustainable Growth and Use. IntechOpen; 2013. pp. 390-399. DOI: 10.5772/55338

[10] Koufopanos CA, Papayannakos N, Maschio G, Lucchesi A. Modelling of the pyrolysis of biomass particles. Studies on kinetics, thermal and heat transfer effects. The Canadian journal of chemical engineering. 1991;**69**(4): 907-915

[11] Wu W, Cai J, Liu R. Isoconversional kinetic analysis of distributed activation energy model processes for pyrolysis of solid fuels. Industrial and Engineering Chemistry Research. 2013;**52**(40): 14376-14383

[12] Gordina NE, Prokof'ev VY, Hmylova OE, Kul'pina YN. Effect of ultrasound on the thermal behavior of the mixtures for the LTA zeolite synthesis based on metakaolin. Journal of Thermal Analysis and Calorimetry. 2017;**129**(3):1415-1427

[13] Guida MY, Bouaik H, ElMouden L, Moubarik A, Aboulkas A, Elharfi K, et al. Utilization of starink approach and avrami theory to evaluate the kinetic parameters of the pyrolysis of olive mill solid waste and olive mill wastewater. Journal of Advanced Chemical Engineering. 2016;**6**:1-8

[14] Luo H, Abu-Omar MM. Lignin extraction and catalytic upgrading from genetically modified poplar. Green Chemistry. 2018;**20**(3):745-753

[15] Xu F, Yu J, Tesso T, Dowell F, Wang D. Qualitative and quantitative analysis of lignocellulosic biomass using infrared techniques: A mini-review. Applied Energy. 2013;**104**:801-809

[16] Rohmawati B, Sya'idah FAN, Alighiri D, Eden WT. Synthesis of bioplastic-based renewable cellulose

acetate from teak wood (*Tectona grandis*) biowaste using glycerol-chitosan plasticizer. Oriental Journal of Chemistry. 2018;**34**(4):1810

[17] Wang G, Li W, Li B, Chen H. TG study on pyrolysis of biomass and its three components under syngas. Fuel. 2008;**87**(4–5):552-558

[18] Mohammed MAA, Salmiaton A, Azlina WW, Amran MSM. Gasification of oil palm empty fruit bunches: A characterization and kinetic study. Bioresource Technology. 2012;**110**: 628-636

[19] Lapuerta MN, Hernández JJ, Rodriguez JN. Kinetics of devolatilisation of forestry wastes from thermogravimetric analysis. Biomass and Bioenergy. 2004;**27**(4):385-391

[20] Hu Y, Wang Z, Cheng X, Ma C. Non-isothermal TGA study on the combustion reaction kinetics and mechanism of low-rank coal char. RSC Advances. 2018;**8**(41):22909-22916

[21] Shuping Z, Yulong W, Mingde Y, Chun L, Junmao T. Pyrolysis characteristics and kinetics of the marine microalgae Dunaliella tertiolecta using thermogravimetric analyzer. Bioresource Technology. 2010;**101**(1): 359-365

[22] Kim YS, Kim YS, Kim SH. Investigation of thermodynamic parameters in the thermal decomposition of plastic waste−waste lube oil compounds. Environmental Science & Technology. 2010;**44**(13): 5313-5317

[23] Vlaev LT, Georgieva VG, Genieva SD. Products and kinetics of non-isothermal decomposition of vanadium (IV) oxide compounds. Journal of Thermal Analysis and Calorimetry. 2007;**88**(3):805-812

[24] Coker AK. Ludwig's Applied Process Design for Chemical and Petrochemical Plants. Burlington, VT, USA: Elsevier, Gulf Professional Publishing; 2014

[25] White JE, Catallo WJ, Legendre BL. Biomass pyrolysis kinetics: A comparative critical review with relevant agricultural residue case studies. Journal of Analytical and Applied Pyrolysis. 2011;**91**(1):1-33

[26] Málek J. The kinetic analysis of non-isothermal data. Thermochimica Acta. 1992;**200**:257-269

[27] Senum GI, Yang R. Rational approximations of the integral of the Arrhenius function. Journal of Thermal Analysis and Calorimetry. 1977;**11**(3): 445-447

[28] Stanko M, Stommel M. Kinetic prediction of fast curing polyurethane resins by model-free isoconversional methods. Polymers. 2018;**10**(7):698

[29] Burnham AK, Weese RK, Weeks BL. A distributed activation energy model of thermodynamically inhibited nucleation and growth reactions and its application to the $\beta-\delta$ phase transition of HMX. The Journal of Physical Chemistry B. 2004;**108**(50): 19432-19441